http://dx.doi.org/10.5012/bkcs.2013.34.1.309

Fluorescence and Fluorescence Excitation Spectroscopy of 5,8-Dihydroxy-1,4-naphthoquinone. Analysis of the Electronic Spectra *via* the Time-Dependent DFT Calculation

Bong Hyun Boo[†,‡,*] and Ji Hwi Kim[†]

[†]*Department of Chemistry, Chungnam National University, Daejeon 305-764, Korea*
[‡]*Departimento di Chimica, Universita degli Studi di Perugia, 06123 Perugia, Italia. [*]E-mail: bhboo@cnu.ac.kr*
Received August 23, 2012, Accepted October 28, 2012

Key Words : 5,8-Dihydroxy-1,4-naphthoquinone, Fluorescence, Fluorescence excitation, TD DFT, Orbital population analysis

Excited-state intramolecular proton transfer (ESIPT) has been a research topic of incessant and wide interest because of its importance in many photophysical,[1] photochemical,[2-4] biological processes,[5,6] and a wide range of application, such as fluorescence molecular probes,[1] luminescent materials,[1] and advanced polymer devices for lasing, optical storage, and electroluminescence.[7] 5,8-Dihydroxy-1,4-naphthoquinone (DHNQ) is one of the simple and ideal molecules for the theoretical elucidation of the photophysical and photochemical processes occurring near the lowest excitation energy. It is quite intriguing to elucidate the molecular orbitals located near the HOMO and LUMO levels in conjunction with specific photochemical processes, and to estimate the intramolecular hydrogen bond strength on the basis of the MO. Ground-state intramolecular proton transfer was studied before, indicating that there are double minima, and the energy to cross over the barrier separating the double minima is found to be high.[8]

The main research goals of the present study are (1) to evaluate the excitation and deactivation behaviors near the UV absorption thresholds by means of the absorption, fluorescence, and fluorescence excitaton spectroscopy; (2) to evaluate the vertical excitation energies with the time-dependent (TD) DFT method which can help to make unambiguous assignment of the electronic spectra; (3) finally to clarify the molecular orbitals associated with the electronic transitions and then to infer the hydrogen bond strength relevant to the MO involved. Reliable reproduction of the electronic excitation spectrum might help to assign unambiguously the excitation, fluorescence, and fluorescence excitation spectra. Also, the orbital population analysis can render the insight into efficiency of proton or hydrogen transfers.

Experimental and Theoretical Methodologies

Conventional spectrometers were used to measure the absorption, fluorescence, and fluorescence excitation spectra of a 2.0×10^{-5} M HDNQ solution in cyclohexane. The ground-state equilibrium geometries and the vibrational frequencies were probed by using the Kohn-Sham DFT.[9] Becke's three-parameter exchange functional[10,11] and the gradient-corrected Lee-Yang-Parr correlational functional (B3LYP)[12] were used with the cc-pVTZ basis set.[13-16] The TD DFT method[17-19] was also applied to compute the vertical excitation energies and to elucidate the corresponding MOs with the B3LYP/cc-pVTZ method at the various S_0 geometries optimized with the B3LYP/cc-pVTZ method. Natural population analysis (NPA) was also performed to give a satisfactory description of the atomic charges and the orbital populations of the molecular wavefunctions. All calculations were carried out with the Gaussian 09 suite of program.[20]

Results and Discussion

We achieved the molecular model of DHNQ in the fundamental state optimized with the B3LYP/cc-pVTZ method under the tight C_{2v} option. No imaginary frequency is found in the frequency calculation, indicating that the structure evaluated in the present study is a global or a local minimum. The absorption spectrum of a 2.0×10^{-5} M DHNQ solution in cyclohexane is shown in Figure 1, and is compared with the simulated absorption spectrum achieved with the TD DFT B3LYP/cc-pVTZ calculation in which 20 vertical excitation energies were evaluated. It is shown in the previous study that the TD DFT B3LYP/cc-pVTZ//B3LYP/cc-pVTZ calculations overestimate within only $6.83 \pm 5.17\%$ the 0_0^0 bands of 13 compounds containing at least one phenyl group.[21] The rms deviation is shown to be low as 0.177 eV.[21] Note that the simulated spectrum shown in Figure 1(b) was shifted to red by using a scaling factor of 0.930, the value used previously.[21] Line spreading of the oscillator strengths was performed by using a Gaussian line shape function having a unique full width at half maximum (fwhm) of 0.1 eV. Note that the fwhm of 0.1 eV is arbitrarily chosen. We found that the broad and smooth spectrum reproduced by using the value for the fwhm mimics the experimental spectrum. Also, note that the fwhm of 0.1 eV does not reveal a physical meaning.

The notations for the simulated electronic absorption spectrum shown in Figure 1(b) refer to the states of the final destinations for the electronic processes. Note that the ground state is 1^1A_1 and the number in front of the state notation indicates the energy order. Therefore, the lowest and the second lowest peaks (two of the three major peaks) appear-

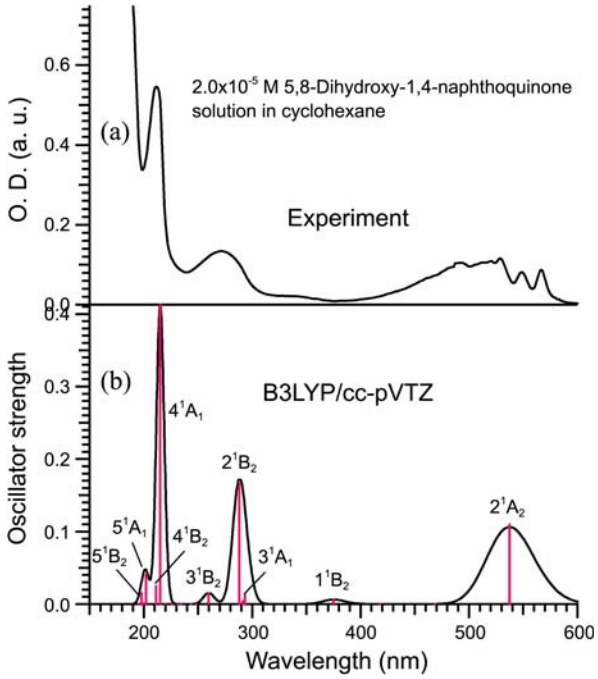

Figure 1. Absorption spectrum measured in a 2.0×10^{-5} M 5,8-dihydroxy-1,4-naphthoquinone solution in cyclohexane is compared with the simulated absorption spectrum calculated with the TD DFT B3LYP/cc-pVTZ//B3LYP/cc-pVTZ method. (a) Absorption spectrum. (b) Simulated absorption spectrum achieved with the TD DFT B3LYP/cc-pVTZ method. The peak assignments refer to the final states.

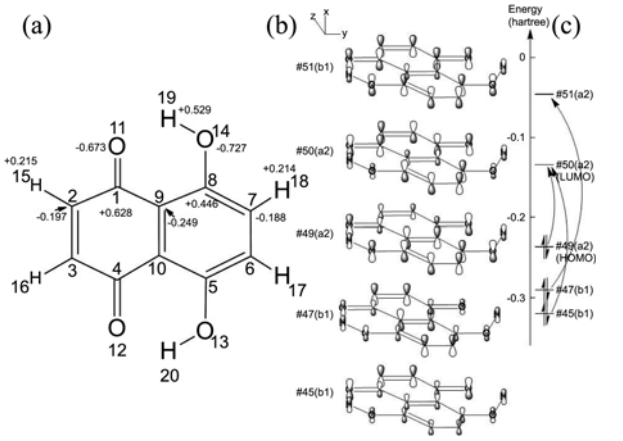

Figure 2. Atomic charges predicted by the natural population analysis with the MP2/cc-pVTZ method and the molecular orbitals near the nonbonding level. (a) The atomic charge and the numbering. (b) The MO revealing the individual coefficients. (c) The MO energy levels.

ing in Figure 1(b) represent $1^1A_1 \rightarrow 2^1A_1$ and $1^1A_1 \rightarrow 1^1B_2$, respectively. Orbital population analysis was performed to provide information about the coefficients of the molecular orbitals which contribute mainly to the excited 2^1A_1, 2^1B_2, and 4^1A_1 states. The TD DFT calculation indicates that the lowest electronic excitation corresponds to the transition from the 49th MO to 50th MO. Note that the 49th MO refers to the HOMO whereas the 50th MO is the LUMO. Figure 2 presents the numbering of the MO and the individual atomic charges evaluated with the MP2/cc-pVTZ method (Fig. 2(a)), and the MO coefficients involved in the principal absorptions (Fig. 2(b)), and also describes the corresponding MO energies (Fig. 2(c)). Interestingly, the MOs, whose energies lie near the nonbonding levels involve only p_x (in here p_π) of the carbon atoms and the hydrogen (of the O-H bonds) atoms. It is intriguing to observe that the MO coefficients of the hydroxy O and H atoms can have the same or the opposite signs relevant to the electronic excitation. The coefficient referring to the micro-configuration (not spin adapted) involving the 49th MO $\rightarrow$ the 50th MO is found to be 0.70730, which is converted to 1, indicating the 100% contribution from the pertinent singlet configuration. Note that if we want the percentage contribution from the pertinent singlet configuration, we must square the coefficient and multiply it by 2 to give 100%. During the transition of the 49th MO $\rightarrow$ the 50th MO, the signs of the coefficients of the p_x orbitals related to the O-H bond are not changed, which might imply that the O-H bond strength is not weakened. We presume that the signs of the O-H and O$\cdots$H MO coefficients determine the intramolecular proton or hydrogen transfer efficiency. This kind orbital population analysis may be informative as to the efficiency of the intramolecular proton or hydrogen transfer.

One of the three major absorptions involves $1^1A_1 \rightarrow 2^1B_2$, attributable to the electronic transition from the 45th MO to the 50th MO with the 73.0% contribution. Figure 2(b) also describes the 45th MO. One of the three major absorptions includes $1^1A_1 \rightarrow 4^1A_1$, arising from the electronic transition from the 47th MO to the 51st MO with the 90.2% contribution. Figure 2(b) also reveals the 47th and 51st MOs.

When we excited the molecule at 460 and 510 nm corresponding to $1^1A_1 \rightarrow 2^1A_1$, the lowest excitation process, the excited singlet species emits slightly red-shifted fluorescence whose spectral shape is found to reveal the mirror image. When we excited the molecule at 380 nm corresponding to $1^1A_1 \rightarrow 1^1B_2$, whose oscillator strength was calculated to be extremely low, the fluorescence intensity turned out to be, however, extremely high. It is intriguing to observe the long-range tail of the fluorescence ranging to 700 nm (Fig. 3(a)). Why does this happen? This is presumably because the excited state intramolecular energy transfer involving the $1^1B_2 \rightarrow 2^1A_1$ transition occurs, which in turn emits the fluorescence. What happened if we excited the molecule at 270 nm? We observed fluorescence spanning three regions corresponding to the fluorescence decays involving the $2^1B_2 \rightarrow 1^1A_1$, $1^1B_2 \rightarrow 1^1A_1$, and $2^1A_1 \rightarrow 1^1A_1$ relaxations. These events can be taken as an indication of the occurrences of the energy transfers competing with those of the corresponding fluorescences.

In an attempt to confirm the mechanistic interpretation of the fluorescence decay processes, we also measured the fluorescence excitation spectra by using the same solution. We found the fluorescent channels emitting the 610- and 670-nm fluorescences when we excited the molecules in the wavelength spanning 250-600 nm. The fluorescence effici-

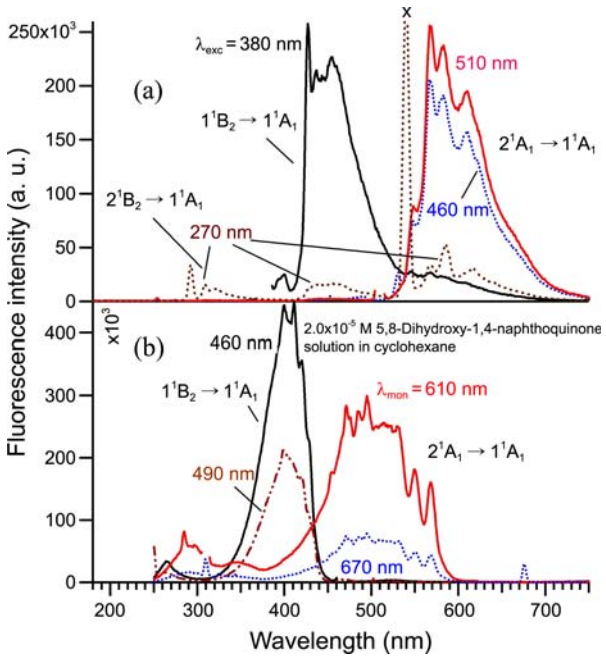

Figure 3. Fluorescence spectra of a 2.0×10^{-5} M 5,8-dihydroxy-1,4-naphthoquinone solution in cyclohexane are compared with the fluorescence excitation spectra measured at the various monitor-ing wavelengths. (a) Fluorescence spectrum. (b) Fluorescence excitation spectrum. The notation of "x" shown in Figure 3(a) indicates the scattered incident light.

ency turns out to be relatively great when we excited the molecule at ≈ 500 nm. This implies that the 2^1A_1 fluorescent states are attained mainly *via* the excitation from the 1^1A_1 state. We also observed a minor channel involving the $1^1A_1 \rightarrow 1^1B_2 \rightarrow 2^1A_1 \rightarrow 1^1A_1$, which was initiated by the photo-absorption at 350 nm (Fig. 3(b)). We also observed another minor channel initiated by the absorption of a UV photon of ≈ 290 nm, which leads to the 1^1A_1 state *via* the $1^1A_1 \rightarrow 2^1B_2 \rightarrow 2^1A_1 \rightarrow 1^1A_1$ consecutive photophysical process.

We observed fluorescent channels emitting the 460- and 490-nm fluorescences, which might be attained by absorbing the ≈ 400-nm photon (Fig. 3(b)). It is interesting to observe a direct photophysical process involving the $1^1A_1 \rightarrow 1^1B_2 \rightarrow 1^1A_1$. This direct fluorescence decay involving the $1^1B_2 \rightarrow 1^1A_1$ process may not conform to the Kasha rule, which states that photon emission occurs in appreciable yield only from the lowest excited state within a given spin multiplicity.[22] A minor channel initiated by the absorption of the ≈ 265-nm photon (Fig. 3(b)) leads to the 460-nm fluorescence, which presumably occurred *via* the $1^1A_1 \rightarrow 3^1B_2 \rightarrow 1^1B_2 \rightarrow 1^1A_1$ photophysical process.

It has been clarified in a literature that natural population analysis (NPA) developed by Reed et al. is an alternative to conventional Mulliken population analysis (MPA), seems to better describe the electron distribution in compounds of high ionic character.[23,24] A previous study by Collins *et al.* also indicates that the MPAs seem to give an unreasonable physical picture of the charge distribution in compounds having high ionic character.[25] The atomic charges of the H-bonded hydrogen atom are found to be much larger than predicted by the Mulliken population analysis. Comparative experimental studies are necessary to clarify the efficiencies of proton and/or hydrogen atom transfers in conjunction with the analysis of the relevant molecular wave functions.

Conclusions

The TD DFT calculation indicates that the lowest electronic excitation corresponding one of the three major peaks is the transition from the 49th to the 50th MO. One of the three major absorptions involves $1^1A_1 \rightarrow 2^1B_2$, attributable to the electronic transition from the 45th MO to the 50th MO. The MOs, whose energies lie near the nonbonding levels, involve only p_x (in here p_π) of the carbon atoms and the hydrogen atoms involving only the hydrogen bonding. When we excited the molecule at 460 and 510 nm, the excitation energies of which correspond to $1^1A_1 \rightarrow 2^1A_1$, the lowest excitation process, the resulting excited singlet species emits slightly red-shifted fluorescence. It is also found that the fluorescence spectral shape reveals the mirror image. The decay channels emitting the 610- and 670-nm fluorescences were found when we excited the molecule in the wavelength range from 250 to 600 nm. The fluorescence efficiency was great when we excited the molecule at ≈ 500 nm. The fluorescence decay channel involving $1^1B_2 \rightarrow 1^1A_1$ is found to be correlated with mainly $1^1A_1 \rightarrow 1^1B_2$. We also observed a minor channel involving the $1^1A_1 \rightarrow 1^1B_2 \rightarrow 2^1A_1 \rightarrow 1^1A_1$ process, which was initiated by the photo-absorption at 350 nm. We also observed a minor $1^1A_1 \rightarrow 2^1B_2$ excitation channel (by absorbing 290 nm) leading to the 610- and 670-nm fluorescences. The observation of the sizable red-shifted fluorescence implies the occurrence of the excited state energy transfer involving the $1^1A_1 \rightarrow 2^1B_2 \rightarrow 2^1A_1 \rightarrow 1^1A_1$ photophysical process. We observed another fluorescent channels emitting the 460- and 490-nm fluorescences, which might be attained by absorbing the ≈ 400-nm photon *via* the $1^1A_1 \rightarrow 1^1B_2 \rightarrow 1^1A_1$ process. A minor channel initiated by the absorption of the ≈ 265-nm photon leads to the 460-nm fluorescence decay channel *via* the $1^1A_1 \rightarrow 3^1B_2 \rightarrow 1^1B_2 \rightarrow 1^1A_1$ photophysical process.

Acknowledgments. This work was supported by the Distinguished Regional Scientist Research Program of the National Research Foundation (NRF) of Republic of Korea (Grant No: NRF-2012-0004484), which is gratefully acknowledged. The author is very grateful to Professor Aquilanti of Department of Chemistry, University of Perugia, Perugia, Italy, who made him to stay comfortably at Perugia in Italy for 6 months and provided valuable help in the quantum mechanical calculation.

References

1. Zhao, J.; Ji, S.; Chen, Y.; Guo, H.; Yang, P. *Phys. Chem. Chem. Phys.* **2012**, *14*, 8803.
2. Stolow, A. *Annu. Rev. Phys. Chem.* **2003**, *54*, 89.

3. Hsieh, C.-C.; Jiang, C.-M.; Chou, P. T. *Acc. Chem. Res.* **2010**, *43*, 1364.
4. Chipem, F. A. S.; Mishra, A.; Krishnamoorthy, G. *Phys. Chem. Chem. Phys.* **2012**, *14*, 8775.
5. Scrutton, N. S.; Groot, M. L.; Heyes, D. J. *Phys. Chem. Chem. Phys.* **2012**, *14*, 8818.
6. Hsieh, C.-C.; Chou, P.-T.; Shih, C.-W.; Chuang, W.-T.; Chung, M.-W.; Lee, J.; Joo, T. *J. Am. Chem. Soc.* **2011**, *133*, 2932.
7. Park, S.; Kim, S.; Seo, J.; Park, Y. S. *Macromol. Res.* **2008**, 16, 385.
8. Yi, P. G.; Liang, Y. H. *Chem. Phys.* **2006**, *322*, 382.
9. Kohn, W.; Sham, L. J. *Phys. Rev. A* **1965**, *140*, 1133.
10. Becke, A. D. *Phys. Rev. A* **1988**, *38*, 3098.
11. Becke, A. D. *J. Chem. Phys.* **1993**, *98*, 5648.
12. Lee, C.; Yang, W.; Parr, R. G. *Phys. Rev. B* **1988**, *37*, 785.
13. Dunning, T. H., Jr. *J. Chem. Phys.* **1989**, *90*, 1007.
14. Kendall, R. A.; Dunning, T. H., Jr.; Harrison, R. J. *J. Chem. Phys.* **1992**, *96*, 6796.
15. Wilson, A. K.; van Mourik, T.; Dunning, T. H., Jr. *J. Mol. Struct.* (*Theochem*) **1996**, *388*, 339.
16. Davidson, E. R. *Chem. Phys. Lett.* **1996**, *260*, 514.
17. Bauernschmitt, R.; Ahlrichs, R. *Chem. Phys. Lett.* **1996**, *256*, 454.
18. Casida, M. E.; Jamorski, C.; Casida, K. C.; Salahub, D. R. *J. Chem. Phys.* **1998**, *108*, 4439.
19. Stratmann, R. E.; Scuseria, G. E.; Frisch, M. J. *J. Chem. Phys.* **1998**, *109*, 8218.
20. Frisch, M. J.; Trucks, G. W.; Schlegel, H. B.; Scuseria, G. E.; Robb, M. A.; Cheeseman, J. R.; Scalmani, G.; Barone, V.; Mennucci, B.; Petersson, G. A.; Nakatsuji, H.; Caricato, M.; Li, X.; Hratchian, H. P.; Izmaylov, A. F.; Bloino, J.; Zheng, G.; Sonnenberg, J. L.; Hada, M.; Ehara, M.; Toyota, K.; Fukuda, R.; Hasegawa, J.; Ishida, M.; Nakajima, T.; Honda, Y.; Kitao, O.; Nakai, H.; Vreven, T.; Montgomery, J. A., Jr.; Peralta, J. E.; Ogliaro, F.; Bearpark, M.; Heyd, J. J.; Brothers, E.; Kudin, K. N.; Staroverov, V. N.; Kobayashi, R.; Normand, J.; Raghavachari, K.; Rendell, A.; Burant, J. C.; Iyengar, S. S.; Tomasi, J.; Cossi, M.; Rega, N.; Millam, J. M.; Klene, M.; Knox, J. E.; Cross, J. B.; Bakken, V.; Adamo, C.; Jaramillo, J.; Gomperts, R.; Stratmann, R. E.; Yazyev, O.; Austin, A. J.; Cammi, R.; Pomelli, C.; Ochterski, J. W.; Martin, R. L.; Morokuma, K.; Zakrzewski, V. G.; Voth, G. A.; Salvador, P.; Dannenberg, J. J.; Dapprich, S.; Daniels, A. D.; Farkas, Ö.; Foresman, J. B.; Ortiz, J. V.; Cioslowski, J.; Fox, D. J. Gaussian 09, Revision A. 1; Gaussian, Inc.; Wallingford CT, 2009.
21. Boo, B. H.; Ryu, S. Y.; Yoon, M.; Koh, S. G.; Park, K. L. *J. Phys. Chem. A* **2010**, *114*, 8969.
22. Kasha, M. *Discuss. Faraday Soc.* **1950**, *9*, 14.
23. Reed, A. E.; Weinstock, R. B.; Weinhold, F. *J. Chem. Phys.* **1985**, *83*, 735.
24. Lee, S. Y.; Boo, B. H.; Kang, H. K.; Kang, D.; Judai, K.; Nishijo, J.; Nishi, N. *Chem. Phys. Lett.* **2005**, *411*, 484.
25. Collins, J. B.; Streitwieser, A. *J. Comput. Chem.* **1980**, *1*, 81.